Down and Up Conversion Luminescence of the Lead-Free Organic Metal Halide Material: $(C_9H_8NO)_2\,SnCl_6\,2H_2O$

Lamia Saidi[*,†], Amira Samet[†],Thameur Dammak[†], Sebastien Pillet[§], and Younes Abid[*,†]

[†]Laboratoire de Physique Appliquée, Université de Sfax, BP 1171, 3018 Sfax, Tunisia
[§] Université de Lorraine, CNRS, CRM2, Nancy, 54506 Vandoeuvre-les-Nancy, France

Corresponding authors
*E-Mail : lamiasaidi93@gmail.com
younes.abid@fss.rnu.tn

ABSTRACT

The present work deals with the optical properties of hybrid organic metal halide material namely $(C_9H_8NO)_2SnCl_6.2H_2O$. Its structure is built up from isolated $[SnCl_6]^{2-}$ octahedral dianions surrounded by Hydroxylquinolinium organic cations $(C_9H_8NO)^+$, abbreviated as $[HQ]^+$. Unlike the usual hybrid materials, where metal halide ions are luminescent semiconductors while the organic ones are optically inactive, $[HQ]_2SnCl_6.2H_2O$ contains two optically active entities: $[HQ]^+$ organic cations and $[SnCl_6]^{2-}$ dianions. The optical properties of the synthesized crystals were studied by optical absorption spectroscopy, photoluminescence measurements and DFT calculations of electronic density of states.
These studies have shown that both organic and inorganic entities have very close HOMO-LUMO gaps and very similar band alignments favoring the resonant energy transfer process. In addition, measurements of luminescence under variable excitations reveal an intense green luminescence around 497 nm under UV excitation (down conversion) and infrared excitation (up conversion luminescence). The down conversion luminescence is assigned to the π-π^* transition within the $[HQ]^+$ organic cations involving charge transfer between the organic and inorganic entities, whereas the up conversion luminescence is on based the triplet-triplet annihilation mechanism (TTA).

1. Introduction

Hybrid organic-inorganic metal halides with the general formula $R_xM_yX_z$ (R: organic group, M: metal and X: halogen) form a large family of interesting hybrid materials due to their structural diversity, optoelectronic properties, as well as their ability to be processed using low temperature techniques. Their structure is characterized by M_yX_z inorganic polyhedra sharing corners, edges or faces to form naturally a large diversity of low dimensional semiconductor networks, surrounded by organic cations through X…H–N hydrogen bonds.[1-6]

During the last decades, the most studied class of hybrid materials is the famous family of perovskites with formula $(RNH_3)_2PbX_4$ and RNH_3PbX_3 .[7-17] Recently, they have attracted a lot of attention thanks to their potential interest for technological applications and for their use in optoelectronic devices[18,19] [19] as well as photovoltaic solar cells.[20-23] More recently, up conversion studies have been also made on this family of materials and have shown rather interesting nonlinear optical properties, namely in colloidal solutions of $MAPbBr_3$ and CsPbBrI nanocrystals.[24-26] The up-conversion phenomenon consists of the combining of two low energy photons in the infrared (IR) region to convert them into higher energy photons (in UV or visible region).[27,28] This property makes this material a promising candidate for the improvement of solar cells' efficiency as it extends the operating spectral range to the infrared (IR) and near infrared (NIR) range. [29-34] So far, the most interesting results were obtained for lead halide based compounds. Taking into account the toxicity of lead (Pb), many researchers have oriented their interest towards the use of other metals such as Cu, Sn and Bi. In this context, we perform in our laboratory several systematic studies on new hybrid metal halides of competitive properties with less toxic metals. As far as we know, only few works have investigated the optical and optoelectronic properties of hybrid metal halides based on $SnCl_6$ framework.[35,36]

In the present work, we will focus on a new lead-free material $[HQ]_2SnCl_6.2H_2O$. The study of photoluminescence under variable excitations shows an intense green luminescence band around 497 nm which appears under both UV excitation (down conversion luminescence) and under infrared excitation (up conversion luminescence). We will show that the down conversion luminescence involves Forster Resonance Energy Transfer (FRET) mechanism[38-40] in which $[SnCl_6]^{2-}$ anions act as donors and $[HQ]^+$ cations act as acceptors, whereas the up conversion luminescence is based on Triplet-Triplet Annihilation (TTA) mechanism.[41-45] This mechanism may generally be described as a conversion of low energy photons in the near infrared region (NIR) into higher energy photons in the visible region: A sensitizer molecule absorbs in (NIR), creating a singlet excited state that undergoes an intersystem crossing (ISC) to the triplet excited state. The energy is then transferred to the triplet state (TET) of another molecule that acts as an emitter (annihilator). Within the emitter, the two triplet excitations fuse into a higher energy singlet excitation and leads to the emission of a higher energy photon in the visible region (Fig. S1). Such a process has the potential to generate substantial improvement of solar conversion efficiency by extending their operating spectral range to the NIR region.[46] Moreover, one should also mention that this material is among the few systems in which the TTA up conversion process occurs without a sensitizer and in which the triplet levels are populated via the transitions from S_0 levels to T levels thanks to the strong interactions between the aromatic rings.[47 48] In addition, almost all of the previous studies on up converter materials have been carried out on colloidal solutions and nanocrystals, [24-28] using intense coherent light excitations (Laser), while our material is among the very few

crystalline up converter materials that operate with non-coherent light and with relatively low intensities.[24-28]

2. Materials and methods

2.1. Crystals Synthesis and Structure Description

Single crystals of $[HQ]_2SnCl_6.2H_2O$ were prepared using the slow evaporation method at room temperature. In the beginning, dissolving (C_9H_7NO) in aqueous HCl solution (37%) gives rise to the (C_9H_8NOCl) organic salt. Later, 1 mmol of the obtained solution was added to 1 mmol of $SnCl_4$ and dissolved in HCl solution (37%). The reaction mixture was then stirred and kept at room temperature. A few weeks later, yellow crystals started to arise.

X-ray diffraction data were collected on a selected single crystal using a Bruker D8 Venture diffractometer equipped with a CMOS PHOTON100 detector, a nitrogen cryostream cooling system, and using MoKα radiation (λ= 0.71073 Å). Data were collected at 100K. The unit-cell determination and data reduction were performed using the APEX2 program suite on the full data set. An empirical absorption correction was performed. The structure was solved by direct methods and successive Fourier difference syntheses, and was refined on F^2 by weighted full-matrix least squares methods using the SHELX-2014 crystallographic software package.[49] All non-H atoms were refined anisotropically. H atoms were located in difference Fourier maps and treated using a riding model, constraining the isotropic displacement parameters to 1.2Ueq of the parent C atom. More details on the structural determination and analysis can be found in the supplementary materials (Tables S1-S3).

CCDC-2069797 contains the supplementary crystallographic data for this paper.

2.2. Density of states calculations

The calculations were based on DFT implemented in the Wien2k package.[50]The interaction between ions and electrons was solved using the modified Becke and Johnson (mbj)[51,52] exchange potential using the all-electron full potential linearized augmented plane wave (FP-LAPW).[53]

Concerning the wave function in the interstitial regions, the cut-off wave value was fixed at $K_{max}= 3/R_{MT,}$ where Kmax is the magnitude of the largest k-vector in the plane wave basis and RMT is the minimum radius of the muffin-tin (MT) spheres. Self-consistency calculation confirmed the energy convergence since the convergence criteria were less than 10^{-3} Ryd per formula unit.

2.3. Optical Measurements

All optical measurements were recorded on single crystals of $[HQ]_2SnCl_6.2H_2O$. Photoluminescence (PL) in addition to excitation photoluminescence (PLE) data were carried out on a Fluoromax-4 spectro fluorimeter equipped with a xenon lamp as an excitation source. Taking into consideration the excitation intensity variation over the whole wavelength range, a calibration ratio is included in the PL measurements. Optical absorption (OA) was measured on the same sample using a UV-vis spectrophotometer (HITACHI, U-3300). An EasyLife-Horiba instrument was employed to measure the photoluminescence lifetime using a 375 nm diode laser as a light source. The time-resolved decay curves were analyzed by a single-exponential iterative fitting program. The temperature-dependent PL spectra were recorded using a Horiba-Jobin Yvon HR 320 spectrometer where the sample was placed in a helium bath cryostat and excited with a 375 nm laser line.

3. Results and discussion

3.1. Crystal structure

$[HQ]_2SnCl_6.2H_2O$ is a zero-periodic hybrid material that crystallizes in the triclinic space group $P\bar{1}$ with a primitive unit cell of dimensions: a = 7.2113(5) Å, b = 9.5272(7) Å and c = 9.5104(7) Å and angles: α = 83.192(2)°, β = 79.981(2)° and γ = 71.109(2)°. As indicated in Fig. 1, its crystal structure is built from isolated $[SnCl_6]^{2-}$ octahedral dianions, located on an inversion center, surrounded by $[HQ]^+$ cations and lattice water molecules. The distortion of the $SnCl_6$ octahedron can be quantitatively evaluated using the quadratic octahedral elongation λ_{oct} and octahedral angle variance σ^2_{oct}:

$$\lambda_{oct} = \frac{1}{6}\sum_{i=1}^{6}(d_i/d_0)^2 \quad \sigma^2_{oct} = \frac{1}{11}\sum_{i=1}^{12}(\alpha_i - 90)^2$$

Where d_i are the six independent Sn–Cl bond lengths, d_0 is the mean Sn–Cl bond length and α_i are the Cl−Sn−Cl angles. The average values of Sn–Cl bond length is 2.4306 Å, leading to negligible octahedral elongation λ_{oct} of 0.9999. The corresponding octahedral angle variance σ^2_{oct} is also very low, evaluated as 0.2026. Such values are very small when compared with reported ones for similar hybrid materials, and reveal the low degree of distortion of the inorganic entity in $[HQ]_2SnCl_6.2H_2O$. The $SnCl_6$ octahedra are arranged as columns stacked along the crystallographic *a* axis with Sn…Sn separation distances of 7.2113(5) Å, without any direct connectivity between neighboring octahedra (Fig. 1); this columnar packing is assisted by Cl…O-H hydrogen bonds through lattice water molecules (shortest dH...Cl = 2.48(3) Å) (Fig. S2). The $[HQ]^+$ cations are stacked parallel to each other through π-π interactions along the crystallographic *a* axis, and form dimers with intra-dimer separation distance of 3.480Å, and inter-dimer separation distance of 3.634Å (Fig. 1(a)). The $[HQ]^+$ cations and $SnCl_6$ octahedra are further connected through O-H…OH_2 (dH...O = 1.85(4) Å),

N-H…OH_2 (dH...O = 1.999(1) Å), and weak C-H…Cl (dH...Cl = 2.7718(5)-2.8927(6) Å) hydrogen bonds.

The crystal structure of the (HQ.Cl) salt has been reported previously.[54] The corresponding crystal packing involves also the formation of dimers of $[HQ]^+$ cations related through π-π interactions with intra-dimer distances of 3.554 Å. These dimers are connected through hydrogen bonds: N-H…Cl (dH...Cl = 2.36(1) Å), C-H…Cl (dH...Cl = 2.74(1) Å) and O-H…OH_2 (dH...O = 1.70(3) Å). We can observe that the intra-dimer distance in the (HQ.Cl) salt is slightly longer than the intra-dimer distance in the hybrid material $[HQ]_2SnCl_6.2H_2O$.

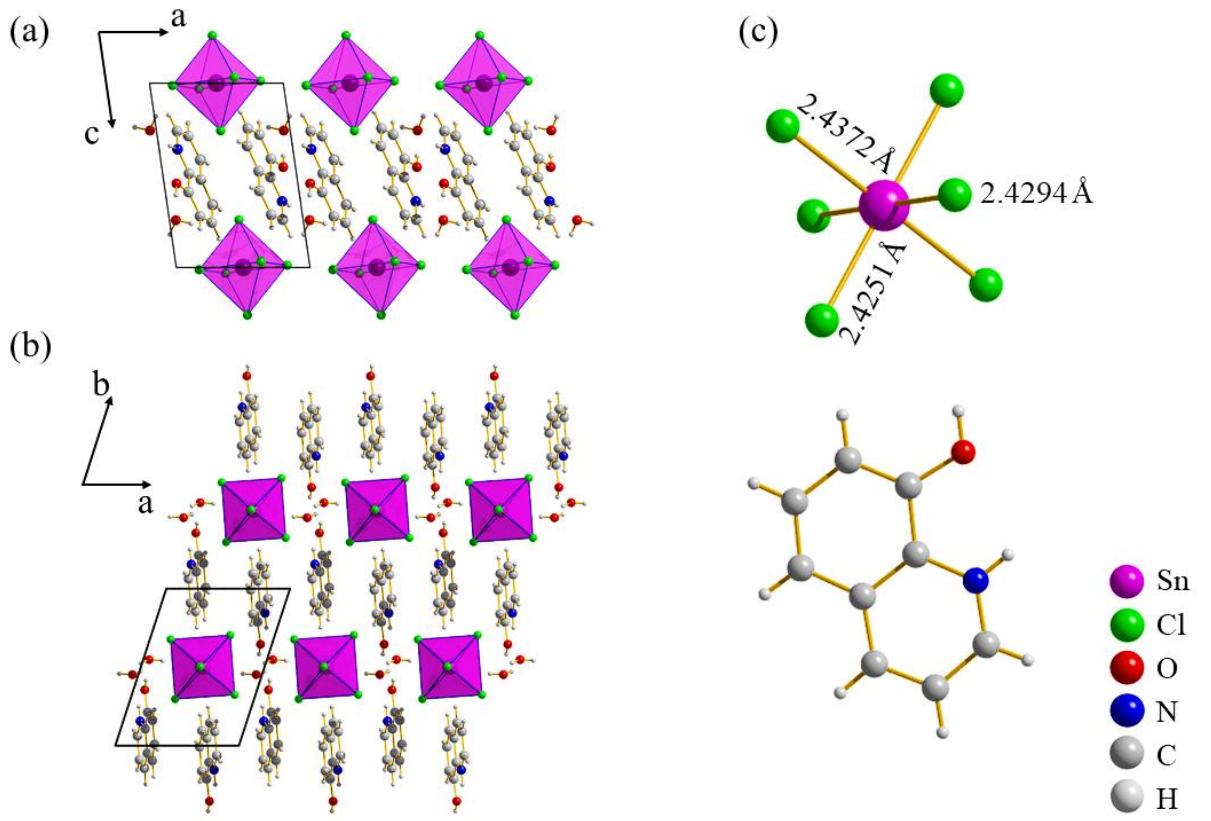

Fig. 1 $[HQ]_2SnCl_6.2H_2O$ crystal structure packing projected along the crystallographic (a) b-axis and (b) c -axis. (c) Molecular design and octahedral coordination of $SnCl_6$.

3.2. Density of states calculations

Given the complexity of the structure and considering the fact that both organic and inorganic species are optically active, a rigorous interpretation and assignment of the optical absorption and photoluminescence spectrum is not so obvious. In such cases, the simulation techniques of the electronic density of states (DOS) prove to be effective tools for a better interpretation of the optical spectra. In this context, we performed theoretical calculations of the DOS in terms of periodic density functional theory (DFT). In Fig. 2, we have illustrated the partial

DOS of each organic and inorganic entity as well as the total DOS. From these results, we can first of all deduce the value of the optical HOMO-LUMO band gap of the title compound estimated at 2.88 eV. Moreover, the analysis of the partial DOS shows that the molecular orbitals of the two organic and inorganic species contribute both to the conduction band and the valence band. Indeed, the valence band (VB) of the title compound mainly originates from N, O and Cl mixed with a small contribution of Sn and C. For the conduction band (CB), it is occupied by nearly the same amount of Sn, Cl, N, O and C.

Furthermore, we notice an alignment of the HOMO-LUMO gaps of the inorganic dianions and the organic cations; they are both estimated nearly at 3 eV. We will see below, in the study by optical spectroscopy that this almost perfect alignment of molecular orbitals and HOMO-LUMO levels of both organic and inorganic parts is in a good agreement with the experimental data, and is in favor of a resonant energy and charge transfer.

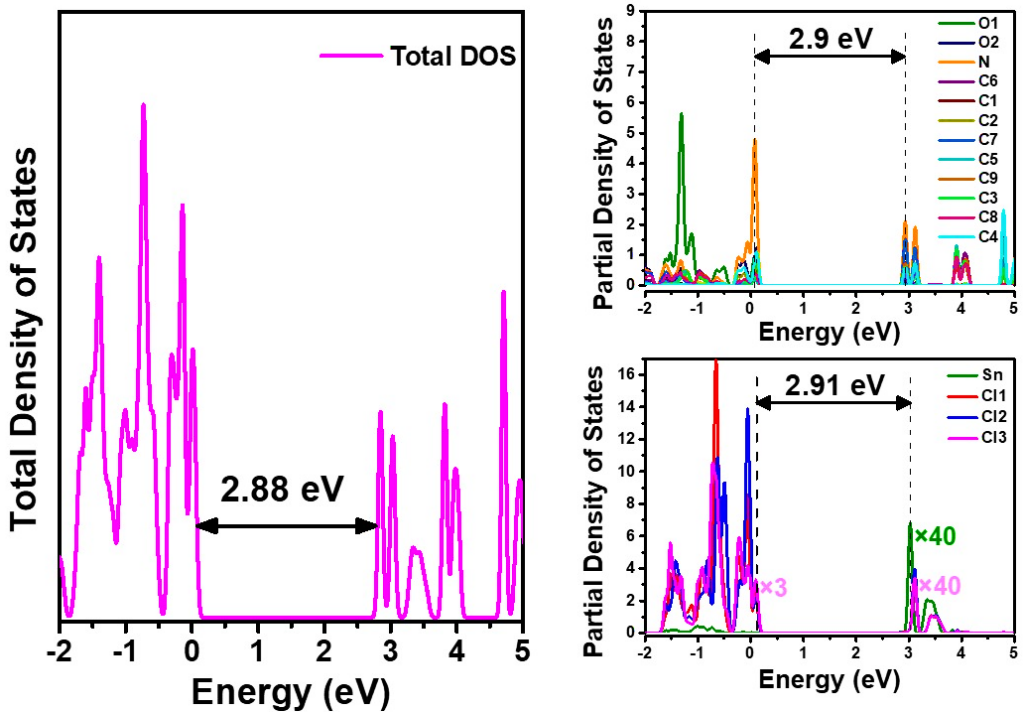

Fig. 2 Calculated partial and total electronic density of states of $[HQ]_2SnCl_6.2H_2O$.

3.3. Optical study

As previously mentioned, our hybrid material includes two luminescent organic and inorganic parts. On the one hand, the inorganic $SnCl_6$ octahedra containing self-trapped excitons which are considered as Wanier type and which depend on the distortion of the octahedra.[55] On the other hand, the organic cations $[HQ]^+$ comprising π-conjugated electrons which can give rise to π-π^* Frenkel exciton.[56] In order to distinguish and analyze the contribution of each

component in the absorption and emission processes, the optical absorption and photoluminescence spectra of the hybrid material were analyzed and interpreted by comparison with the spectra of the organic salt (HQ.Cl) on the one hand and those of Cs_2SnCl_6[57] on the other hand. As we can see in Fig. 3(a), the optical absorption spectra of the organic salt and the hybrid material indicate that they absorb in the same spectral range between 300 and 450 nm, which is in perfect agreement with the results predicted by the theoretical simulations of the electronic density of states which showed an alignment of the HOMO-LUMO energy levels of the organic and inorganic parts.

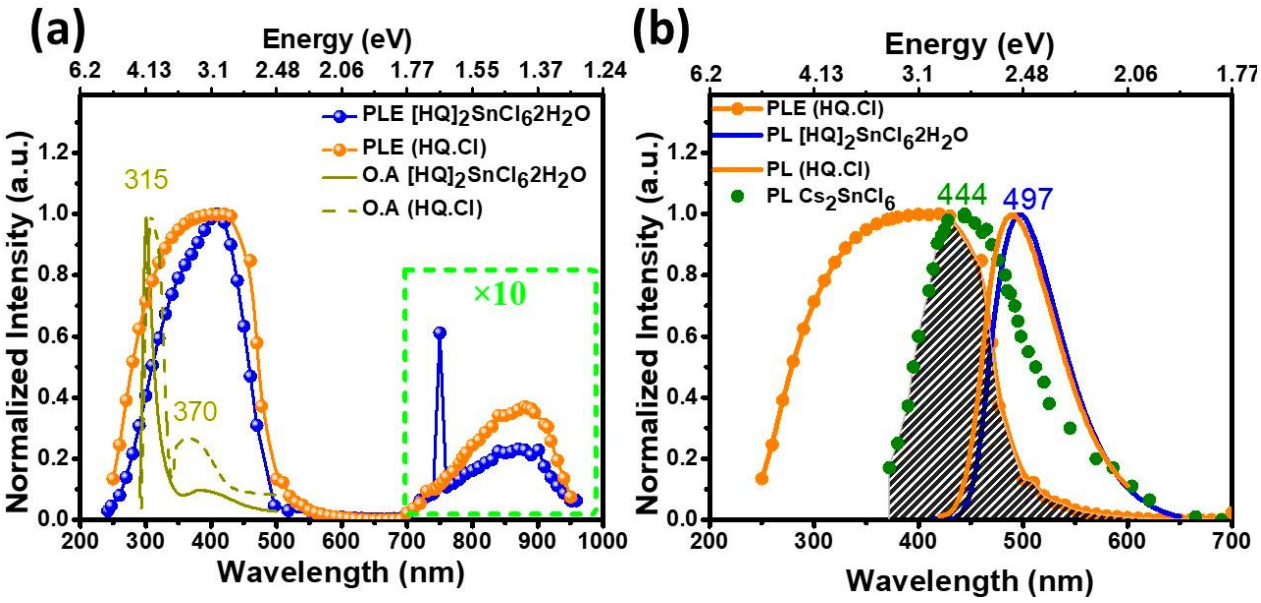

Fig. 3 (a) Room temperature PLE recorded under 490 nm excitation and optical absorption OA of $[HQ]_2SnCl_6.2H_2O$ and (HQ.Cl) salt. (b) Room temperature PL spectra of $[HQ]_2SnCl_6.2H_2O$ and (HQ.Cl) salt compared to the PL spectrum of Cs_2SnCl_6.[57] The dashed area illustrates the overlap between the donor emission ($SnCl_6$) and the acceptor excitation.

These results are also in agreement with the PLE measurements recorded under 490 nm, which showed two spectra of the same shape for the organic and inorganic entities centered at 410 nm (3.02 eV). Moreover, under UV excitation of 375nm, the organic salt as well as the hybrid material show a very intense green emission which can be observed even with the naked eye. In the photoluminescence spectra (Fig. 3(b)), these emissions are characterized by broad and intense bands around 491nm and 497nm for the organic salt and the hybrid respectively. This emission band is unambiguously associated with the electronic π-π^* transition within the organic cations.

We should also point out that in previous studies on tin chloride-based materials,[36,58] in particular on Cs_2SnCl_6[57], the PL spectrum is characterized by a wide emission band around 444 nm associated with exciton recombination in $SnCl_6$ octahedra (Fig. 3 (b)). In the case of

our hybrid material, this band is not observed. This can be explained by the fact that these excitons are quenched by the energy and charge transfer process that can occur between the $SnCl_6$ octahedra and the [HQ] organic cations (RET).

To boost our assumption, we have performed time resolved PL measurements on the organic salt and on the hybrid under 375 nm excitation (Fig. S3). The measured lifetimes are fitted using the following exponential function:

$$I(t) = A \times exp(-t / \tau)$$

where τ is the exciton lifetime and A is the amplitude.[59,60] For our material, the average lifetime is estimated at 30 ns which is comparable with that of the (HQ.Cl) salt; 24 ns, while for self-trapped exciton in other reported $SnCl_6$ based materials, the lifetimes are hundreds of times higher.[55,61,62] This confirms again that the observed luminescence bands are associated with the organic exciton.

Let us now return to the resonant energy/charge transfer (RET). RET[63] can be described as a dipolar interaction between two molecular species (a donor D and an acceptor A) depending essentially on three conditions:

(i) The HOMO-LUMO gap of the acceptor A is less than or equal to that of the donor D.

(ii) The distance between D and A does not exceed a few nm and the transfer process is all the more favored the closer these entities are.

(iii) The donor's emission band must have a significant overlap with the acceptor's absorption band.

For the present case, these three conditions are perfectly satisfied. So that:

(i) DFT calculation and absorption measurements showed an alignment of the HOMO-LUMO gap and molecular orbitals of the two organic inorganic entities.

(ii) The structural study showed that the distance between the organic cation and the $SnCl_6$ octahedra does not exceed 3 Å.

(iii) Fig. 3 (b) shows a significant overlap of the absorption of the organic cation with the emission band of $SnCl_6$.

The data available so far typically characterize the mechanism of resonant energy and charge transfer and may explain the quenching of the inorganic excitons. Moreover, in similar systems this transfer mechanism is described as the conversion of an inorganic exciton to an organic exciton[64] (Fig. S4).

Moreover, it is well known that in hybrid materials, the inorganic excitons and the organic excitons have different thermal behaviors. Indeed, the inorganic excitons assumed as Wannier excitons are very sensitive to the lowering of temperature and the intensity of their PL bands increases considerably, while for organic excitons, the intensity of the PL is much less sensitive to the temperature variation.[12,65-67] In this context, and in order to perform a thermal characterization of the charge transfer between the organic and inorganic parts, we carried out

a temperature-dependence study of the photoluminescence for the hybrid material as well as for the organic salt. The Fig. 4 shows the evolution of the PL spectra of the two compounds in the temperature range 20-300K. As we can see, despite the fact that in the two compounds the photoluminescence originates from the organic cation, they show different thermal behaviors, so that, by lowering the temperature from 300 to 20K, the intensity of the PL band of the hybrid is multiplied by a ratio $R_{Hybrid} = I_{20} / I_{300} = 2.3$. While for the organic salt, the intensity remains almost constant ($R_{Salt} = I_{20} / I_{300} = 1.3$). This perfectly characterizes the charge transfer mechanism which enhances the emission process in the hybrid. Such behavior has been observed in many previous studies and has often been described as the conversion of an inorganic exciton (Wannier) into an organic exciton[12,65-67] (Frenkel).

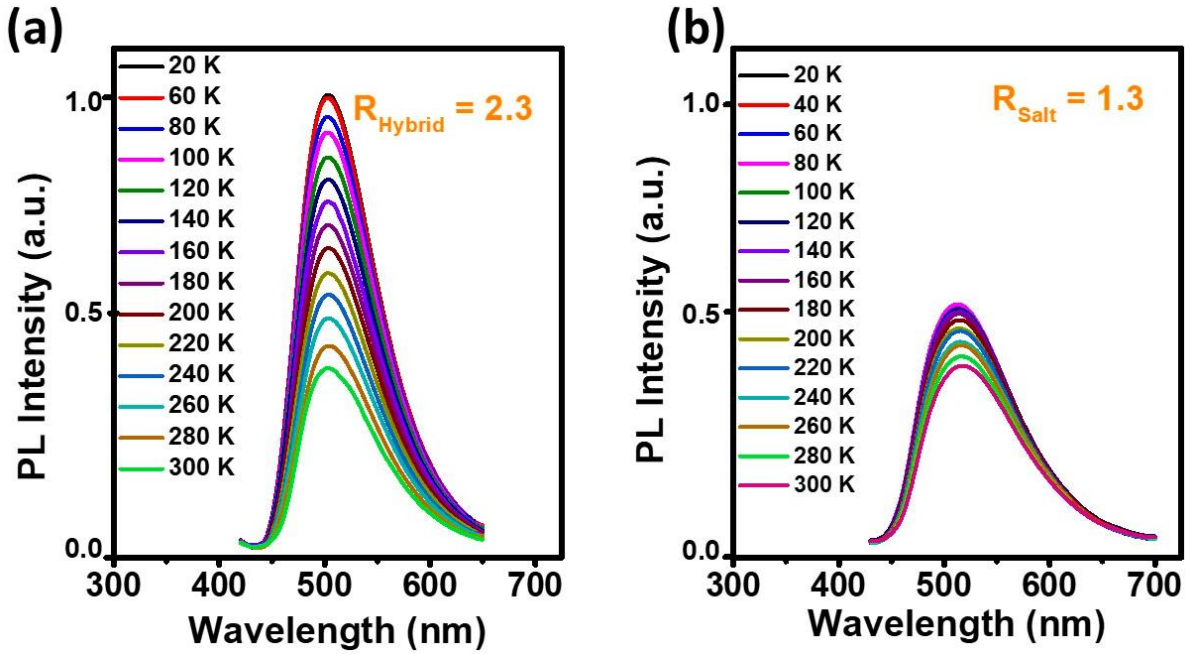

Fig. 4 (a-b) Temperature dependence PL of $[HQ]_2SnCl_6.2H_2O$ and the (HQ.Cl) salt respectively measured under 375 nm excitaion.

In order to investigate the stability of the exciton in the title compound, we plotted the integrated PL intensity as a function of $1/K_BT$, where K_BT is Boltzmann energy (Fig. 5 (a)). The intensity can be fitted using the Arrhenius-type model[68, 69] described as:

$$I_{PL}(T) = \frac{I_0}{1 + a\exp(-\frac{E_a}{K_B T})}$$

Where $I_{PL}(T)$ is the integrated PL intensity at temperature T, I_0 is the integrated PL intensity at 0 K, E_a is the activation energy attributed to the thermally activated non-radiative process. The appropriate fitting parameters lead to an activation energy E_a = 41 meV which is close to

the activation energy of previous studies on homologous materials namely (AMPS)[$SnCl_6$]H_2O (30 meV).[35] This low exciton binding energy suggests that the interaction of free exciton is the dominant in the material unlike other hybrid materials presenting an important activation energy

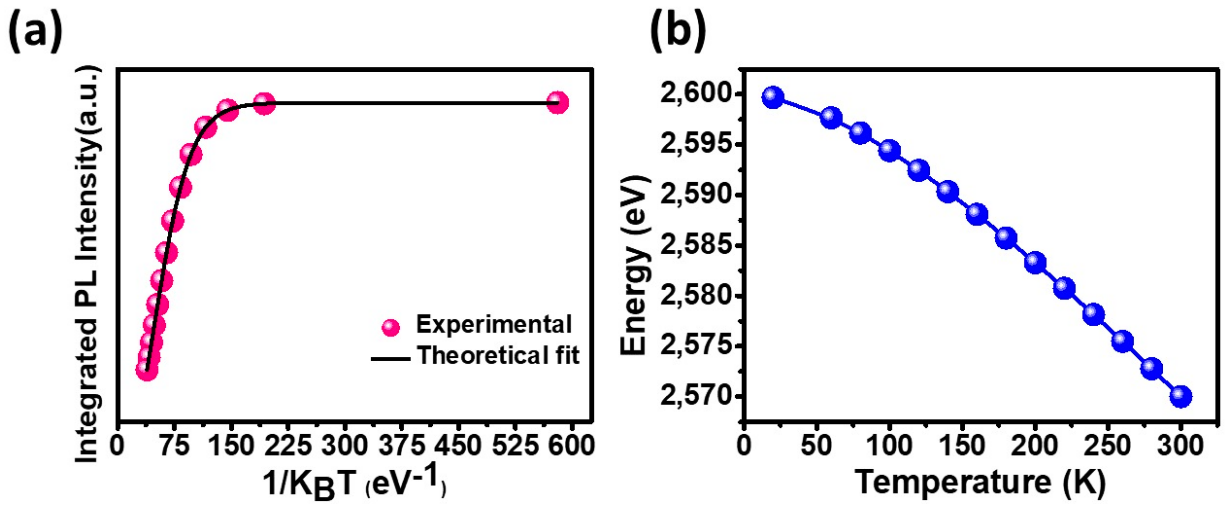

Fig. 5 (a) Temperature dependence of the PL integrated intensity of $[HQ]_2SnCl_6.2H_2O$. (b) PL peak energy as a function of temperature of $[HQ]_2SnCl_6.2H_2O$.

reaching hundreds of meV.[70] It may be also assigned to the stability of the exciton making it visible at room temperature.[71]

As seen in Fig. 5 (b), we have plotted the exciton peak energy in the temperature range from 20 to 300 K to strengthen our confidence in the existence of free exciton behavior. This variation follows the classical Varshni's model[72] described as:

$$E_{ex} = E_{0,ex} - \frac{\alpha T^2}{(\beta + T)}$$

Where $E_{0,ex}$ is the exciton energy at 0 K, α is related to the linear shift of $E_{ex}(T)$ and β is close to the Debye temperature. Effectively, no deviation from this model was detected which is in good agreement with the small activation energy value calculated previously.

In order to better understand the mechanism of energy and charge transfer in our compound, we performed photoluminescence measurements using various excitation energies, covering the UV-visible and near infrared region (300nm- 900nm). Surprisingly, it turned out that the luminescence peak around 497nm is not only obtained for the blue-UV excitation (down conversion), but also for the excitations in the near infrared region (750nm-900nm). As can be seen in Fig. 6 (a), for excitation wavelengths between 250 nm and 500 nm we observe the luminescence band is intense and reaches the maximum intensity around 400 nm and drops of

steeply for excitations between 500 and 700 nm. For excitation range between 700 and 1000 nm, the PL peak reappears and reaches its maximum under excitation around 855 nm. The same study was also carried out on the organic salt. As seen in the Fig. 6 (b) and (c) the comparison between the organic salt and the hybrid materials showed a similar behavior in the two regimes (down conversion and up conversion luminescence).It is worthy to note an enhancement in the hybrid's PL intensity compared to the organic salt's PL intensity. This can be explained by the RET mechanism given that the intensity of the PL band of the hybrid is almost the double of the organic salt in down conversion and almost four times in the up conversion one.

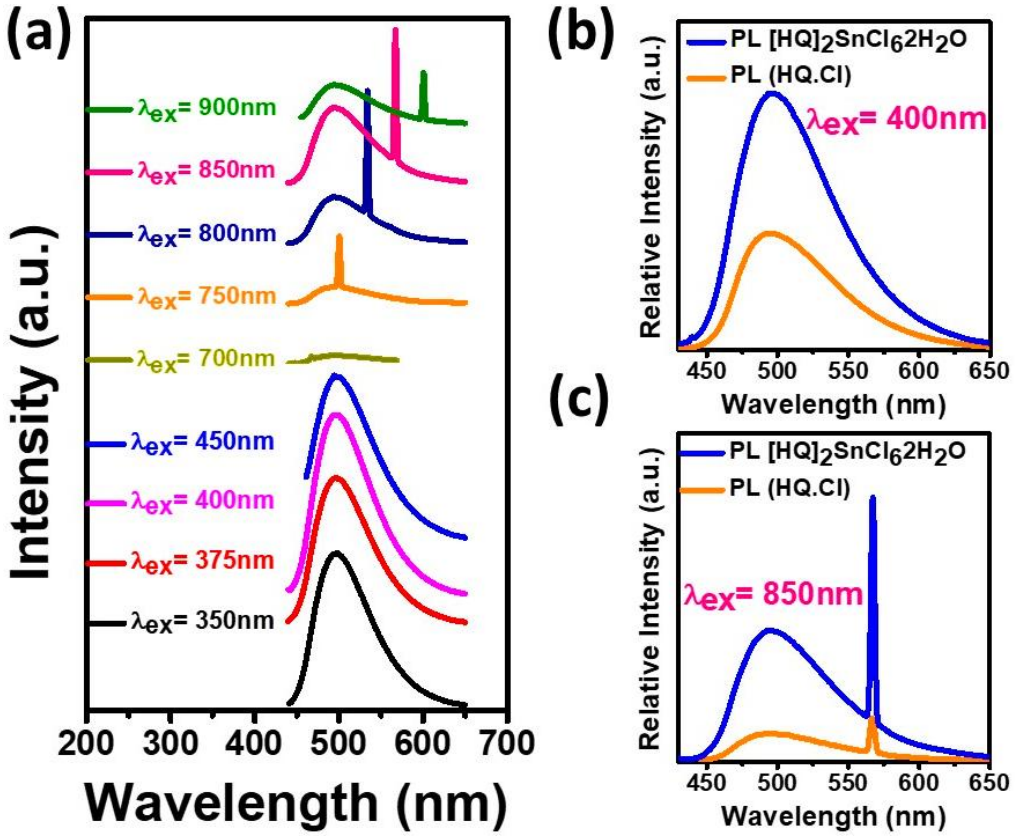

Fig. 6 (a) PL spectra of $[HQ]_2SnCl_6.2H_2O$ under different excitations. (b-c) Relative PL spectra of $[HQ]_2SnCl_6.2H_2O$ and the (HQ.Cl) salt under 400 nm and 850 nm respectively. In (a) all measurements were multiplied by a calibration ratio taking into account the excitation power variation with the excitation wavelength.

The analysis of these data lead to the following deductions:

(i) In both regimes, down and up conversion, the luminescence originates mainly from the organic cation.

(ii) The TTA - UC process occurs without a sensitizer, as the Cl^- and $[SnCl_6]^{2-}$ ions do not have singlet or triplet levels that can take up in the IR and NIR regions.

It seems that among the sensitizer free mechanism, the process of IR photon absorption followed by triplet-triplet annihilation perfectly describes this up conversion process. It is however useful to remember that this process (sketched in Fig. 7) is described as a bimolecular process[73-76] which takes place between two organic species comprising aromatic rings, and occurs in two steps: First, under infrared irradiation, two organic cations $(cation)_1$ and $(cation)_2$ absorb each a photon so that both transit from the S_0 level to the T level. This optical transition, which is theoretically forbidden, becomes allowed thanks to the strong interaction between the two cations. In a second step, the two strongly correlated triplet levels (T, T) fuse into a singlet S_1 level of double energy. This S_1 level can relax at the lower levels via two mechanism: the return to the fission of the S_1 singlet level into two triplet levels (T, T), or the transition to the S_0 level which gives rise to the delayed luminescence that we observed in the visible region (around 497 nm).

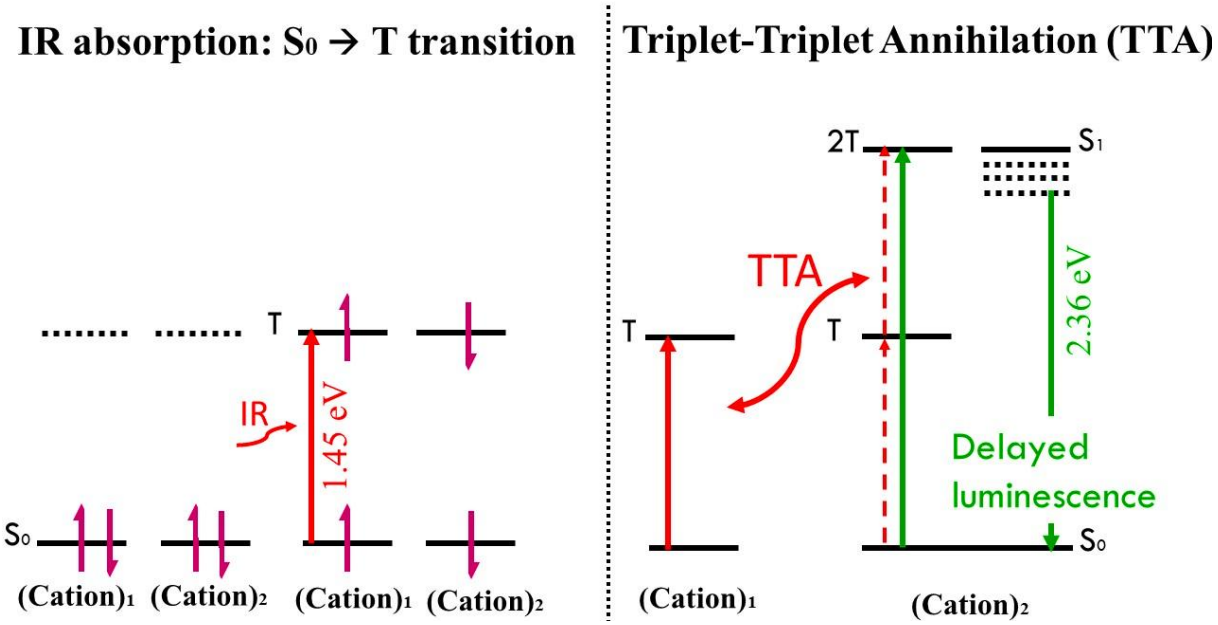

Fig. 7 Schematic illustration of the sensitizer free TTA mechanism: two triplet levels of two interacting cations are populated through the singlet to triplet transition occurring while the absorption of two IR photons. This process is then followed by up conversion luminescence via triplet–triplet annihilation (TTA).

In recent studies carried out on numerous organic systems involving TTA processes it has been demonstrated that this mechanism is mainly dependent of the following criteria:

(i) The molecules involved in this process must have at least two aromatic rings and have a triplet level of energy almost equal to half the energy of the singlet level.

(ii) The stacking of aromatic rings and their interaction facilitate the population of T levels via S_0 → T transitions.

(iii) The transfer of the triplet exciton from one molecule to another is of Dexter type[77] which consists of an exchange of electrons at short distances not exceeding 1 nm.

All these criteria are indeed perfectly satisfied for both the organic salt and the hybrid material:

(i) The quinolinium cation $[HQ]^+$ has two aromatic rings and is endowed with a triplet energy level equal to almost half the singlet energy levels (2.91 eV, 426 nm) of (1.45 eV, 850 nm)

(ii) The crystal structure determined by XRD showed that the organic cations are associated in dimers and their interaction favors the TTA process.

(iii) The interaction distances between two cations determined by DRX are of the order of 3.5 and 3.6 Å. They allow the overlap of wave functions between neighboring molecules to facilitate Dexter transfer. All these results are in good agreement with those found for homologous material $(HQ)_2ZnCl_4$ [54] and other organic crystal systems such as pentacene[78] tetracene[79] or solid organic polymers based on tiophène.[80]

4. Conclusion

This work reports on the optical properties of a new lead free organic hybrid crystals $[HQ]_2SnCl_6.2H_2O$ in which, the two chromophore components $[HQ]^+$ and $[SnCl_6]^{2-}$ have quite close HOMO-LUMO gaps. The study of the photoluminescence with various excitation showed an intense emission signal around 497nm that can be observed under UV excitation (down conversion) or under NIR excitation (up conversion). The comparison with the salt (HQ.Cl) and with the homologous materials showed that the down conversion luminescence involves a resonant energy transfer mechanism in which $[SnCl_6]^{2-}$ acts as a donor and $[HQ]^+$ acts as an acceptor, whereas the up-conversion luminescence is governed by the sensitizer-free triplet- triplet annihilation (TTA). This property makes this material a promising candidate for the improvement of solar cells' efficiency as it has extended the conversion of infrared light to a wider spectral range. Given the band gap tunability depending on the nature of the organic molecule, this opens a new pathway for improving solar cells' performance. Moreover, this up-conversion material can be a good candidate for biological imaging applications. Therefore, we believe that this work will enrich this class of materials by arousing a renewed research on low cost, eco-friendly raw materials, with facile synthesis and excellent optical properties at room temperature.

Conflicts of interest

The authors declare no conflict of interest.

Acknowledgements

This work was supported by the ERANET MED project HYDROSOL, the Ministry of Higher Education of Tunisia and CNRS, French PIA project ‘‘Lorraine Université d’Excellence’’, reference ANR-15-IDEX-04-LUE.

References

1 Mitzi, D. B. Chem. Mater. 1996, **8** (3), 791−800.
2 Billing, D. G., Lemmerer, A. Acta Crystallogr C. 2004, **60** (5), m224-6.
3 Fujisawa, J.; Ishihara, T. Phys. Rev. B 2004, **70** (20), 205330.
4 Samet, A.; Ahmed, A. B.; Mlayah, A.; Boughzala, H.; Hlil, E. K.; Abid, Y. Journal of Molecular Structure, 2010, **977**(1-3), 72–77.
5 Mitzi, D. B. J. Chem. Soc., Dalton Trans. 2001, (1), 1–12.
6 Dammak, T.; Boughzala, H.; Mlayah, A.; Abid, Y. J. Lumin. 2016, **173**, 213–217.
7 Elleuch, S.; Lusson, A.; Pillet, S.; Boukheddaden,K.; Abid,Y. ACS Photonics 2020, **7**, 1178−1187.
8 Zhang, W.-F.;Pan, W.-J.; Xu, T.; Song, R.-Y.;Zhao, Y.-Y.; Yue, C.-Y.; Lei, X. W. Inorganic Chemistry 2020, **59** (19), 14085-14092.
9 Medhioub, O.; Barkaoui, H.; Samet, A.; Pillet, S.; Triki, S.; Abid, Y. J. Phys. Chem. C 2019, **123**(43), 26547–26553.
10 Yangui, A.; Garrot, D.; Lauret, J. S.; Lusson, A.; Bouchez, G.; Deleporte, E.; Pillet, S.; Bendeif, E. E.; Castro, M.; Triki, S.; et al. J. Phys. Chem. C 2015, **119** (41), 23638−23647.
11 Samet, A.; Triki, S.; Abid, Y. J. Phys. Chem. C 2019, **123** (10), 6213-6219.
12 Barkaoui, H.; Abid, H.; Yangui, A.; Triki, S.; Boukheddaden, K.; Abid, Y. J. Phys. Chem. C 2018, **122**, 24253−24261.
13 Hu, T.; Smith, M. D.; Dohner, E. R.; Sher, M.-J.; Wu, X.;Trinh, M. T.; Fisher, A.; Corbett, J.; Zhu, XY.; Karunadasa, HI.; Lindenberg, A. M. J. Phys. Chem. Lett. 2016, **7**(12), 2258–2263.
14 Yin, J.; Li, H.; Cortecchia, D.; Soci, C.; Bredas, J.-L. ACS Energy Lett. 2017, **2**(2), 417–423.
15 Muljarov, E. A.; Tikhodeev, S. G.; Gippius, N. A.; Ishihara, T. Phys. Rev. B 1995, **51**(20), 14370–14378.
16 Mitzi, D. B.; Chondroudis, K.; Kagan, C. R. Inorg. Chem. 1999, **38** (26), 6246–6256.
17 Yu, Z.; Yu, W.; Xing, J.; Ganeev, R. A.; Xin, W.; Cheng, J.; Guo, C. ACS Photonics 2018, **5**, 1619−1627.
18 Manser, J. S.; Christians, J. A.; Kamat, P. V. Chem. Rev. 2016, **116**, 12956−13008.
19 Colella, S.; Mazzeo, M.; Rizzo, A.; Gigli, G.; Listorti, A. J. Phys. Chem. Lett. 2016, **7**(21), 4322–4334.

20 Burschka, J.; Pellet, N.; Moon, S.-J.; Humphry-Baker, R.; Gao, P.; Nazeeruddin, M. K.; Grätzel, M. Nature 2013, **499**(7458), 316–319.
21 Heo, J. H.; Im, S. H.; Noh, J. H.; Mandal, T. N.; Lim, C. S.; Chang, J. A.; Lee, Y. H.; Kim, H. J.; Sarkar, A.; Nazeeruddin, M. K.; Grätzel, M.; Seok, S. I. Nature Photonics 2013, **7**(6), 486-491.
22 Kojima, A.; Teshima, K.; Shirai, Y.; Miyasaka, T. J. Am. Chem. Soc. 2009, **131**(17), 6050–6051.
23 Yang, W. S.; Park, B. W.; Jung, E. H.; Jeon, N. J.; Kim, Y. C.; Lee, D. U.; Shin, S. S.; Seo, J.; Kim, E. K.; Noh, J. H.; Seok, S. I. Science 2017, **356**(6345), 1376-1379.
24 Bagherzadeh-Khajehmarjan, E.; Mirershadi, S.;Ahmadi-Kandjani, S. Appl. Phys. B 2017, **123**(10), 257.
25 Han, Q.; Wu, W.; Liu, W.; Yang, Y. RSC Adv. 2017, **7**, 35757.
26 Han, Q.; Wu, W.; Liu, W.; Yang, Q.; Yang, Y. Optical Materials 2018, **75**, 880–886.
27 Huang, Z. ; Li, X.; Mahboub, M. ; Hanson, K. M. ; Nichols, V. M. ; Le, H. ; Tang, M.L.; Bardeen, C. J. Nano Lett. 2015, **15**(8), 5552–5557.
28 Wieghold, S.; Bieber, A. S.; VanOrman, Z. A.; Daley, L.; Leger, M.; Correa-Baena, J.-P.; Nienhaus, L. Matter. 2019, **1**, 705–719.
29 Nagai, A.; Miller, J. B.; Kos, P.; Elkassih, S.; Xiong, H.; Siegwart, D. J. ACS Biomater. Sci. Eng. 2015, **1**, 1206−1210.
30 Trupke, T.; Green, M. A.; Würfel, P. J. Appl. Phys. 2002, **92**(7), 4117.
31 Bubb, D. M.; Cohen, D.; Qadri, S. B. Appl. Phys. Lett. 2005, **87**, 131909.
32 Som, T.; Karmakar, B. J. Opt. Soc. Am. B 2009,**26**, B21-B27.
33 Zhang, M.; Liu, Y.; Yu, H.; Yu, J.; Zheng, X.; Ai, F.; Pan, X.; Zhao, H.; Tang, M.; Wen, H.; Grai, L.; Mao, Z.; Wang, C. Opt. Mater. Express 2015, **5**, 676-683.
34 Borisov, S. M.; Larndorfer, C.; Klimant, I. Adv. Funct. Mater. 2012, **22**(20), 4360–4368.
35 Dammak, T.; Abid, Y. Opt. Mater.2017,**66**, 302-307.
36 Feddaoui, I.; Abdelbaky, Mohammed S.M.; García-Granda, S.; Essalah, K.; Ben Nasr, C.;Mrad, M.L. J. Mol. Struct. 2019,**1186**, 31-38.
37 Förster T. Ann. Phys. 1948, **437**(1-2), 55–75.
38 Park, Y. R.; Lee, Y.-J.; Yu, C.-J.; Kim, J.-H. J. Appl. Phys. 2010, **108**(4), 044508.
39 Zhang, Q.; Atay, T.; Tischler, J. et al. Nature Nanotech 2007, **2**, 555–559.
40 Shannon, R. D. Acta Cryst. A 1976, **32**, 751–767.
41 Dzebo, D.; Börjesson, K.; Gray, V.; Moth-Poulsen, K.; Albinsson, B. J. Phys. Chem. C 2016, **120**(41), 23397−23406.
42 Gray, V.; Börjesson, K.; Dzebo, D.; Abrahamsson, M.; Albinsson, B.; Moth-Poulsen, K. J. Phys. Chem. C 2016, **120**(34), 19018−19026.

43 Turshatov, A.; Busko, D.; Avlasevich, Y.; Miteva, T.; Landfester, K.; Baluschev, S. Chem.Phys.Chem. 2012, **13**, 3112 – 3115.

44 Singh-Rachford, T. N.; Castellano, F. N. Chem. Rev. 2010,**254**, 2560−2573.

45 Hoseinkhani, S.; Tubino, R.; Meinardi, F.; Monguzzi, A. Chem. Phys. 2015, **17**, 4020−4024.

46 Monguzzi, A.; Borisov, S. M.; Pedrini, J.; Klimant, I.; Salvalaggio, M.; Biagini, P.; Melchiorre, F.; Lelii. C.; Meinardi, F. Adv. Funct. Mater. 2015, **25**(35), 5617–5624.

47 Sasaki, Y.; Amemori, S.; Kouno, H.; Yanai, N.; Kimizuka, N. J. Mater. Chem. C 2017, **5**, 5063—5067.

48 Qiao, X.; Ma, D. Materials Science and Engineering: R 2019, 100519.

49 Sheldrick, G. M. Acta Cryst. 2015, C71, 3-8.

50 Schwarz, K.; Blaha, P.; Madsen, G. K. H. Comput. Phys. Commun. 2002, **147** (1−2), 71−76.

51 Tran, F.; Blaha, P. Phys. Rev. Lett. 2009, **102**(22),226401.

52 Becke, A. D.; Johnson, E. R. A. J. Chem. Phys. 2006,**124**, 221101.

53 Madsen, G. K. H.; Blaha, P.; Schwarz, K.; Sjöstedt, E.; Nordström, L. Phys. Rev. B 2001, **64** (19), 195134.

54 Samet, A.; Pillet, S.; Abid, Y. Phys. Chem. Chem. Phys. 2020, **22**, 1575-1582.

55 Zeng, R., Bai, K., Wei, Q. et al. Nano Res. 2021, **14**, 1551–1558.

56 Frenkel, J. Phys. Rev. 1931, **37** (1), 17−44.

57 Veronese, A.; Patrini, M.; Bajoni, D.; Ciarrocchi, C.; Quadrelli, P.; Malavasi, L. Front Chem. 2020, **8**: 35.

58 BelhajSalah, S.; Abdelbaky, M. S. M.; García-Granda, S.; Essalah, K.; Ben Nasr, C.; Mrad, M. L. J. Mol. Struct. 2018, **1152**, 276–286.

59 Vial, J. C.; Bsiesy, A.; Gaspard, F.; Herino, R.; Ligeon, M.; Muller, F.; Romestain, R.; Macfarlane, R. M. Phys. Rev. B: Condens. Matter Mater. Phys. 1992, **45**(24), 14171−14177.

60 Kobitski, A. Yu.; Zhuravlev, K. S.; Wagner, H. P.; Zahn, D. R. T. Phys.Rev. B. 2001, **63**, 115423: 1-5.

61 Zhang, H., Zhu, L., Cheng, J., Chen, L., Liu, C., Yuan, S. Materials 2019, **12**, 1501.

62 Tan, Z. ; Li, J. ; Zhang, C. ; Li, Z. ; Hu, Q. ; Xiao, Z et al. Adv. Funct. Mater.2018, **28**(29), 1801131.

63 L. Stryer, Annu. Rev. Biochem. 1978, **47**, 819.

64 Blumstengel, S.; Sadofev, S.; Xu, C.; Puls, J.; Henneberger, F. Phys. Rev. Lett. 2006, **97** (23), 237401.

65 Morimoto, K.; Matsuishi, K. J. Phys. Conf. Ser. 2010, **215** (1), 012044.

66 Braun, M.; Tuffentsammer, W.; Wachtel, H.; Wolf, H. C. Chem. Phys. Lett. 1999, **303** (1−2), 157−164.

67 Mitzi, D. B.; Chondroudis, K.; Kagan, C. R. Inorg. Chem. 1999, **38** (26), 6246−6256.

68 Jing, P.; Zheng, J.; Ikezawa, M.; Liu, X.; Lv, S.; Kong, X.; Zhao, J.; Masumoto, Y. J. Phys.Chem. C 2009, **113** (31), 13545−13550.
69 Valerini, D.; Cretí, A.; Lomascolo, M.; Manna, L.; Cingolani,R.; Anni, M. Phys. Rev. B: Condens. Matter Mater. Phys. 2005, **71** (23), 235409.
70 Hong, X.; Ishihara, T.; Nurmikko, A. V. Phys. Rev. B:Condens. Matter Mater. Phys. 1992, **45**, 6961−6964.
71 Trabelsie, S.; Samet, A.; Dammak, H.; Michaud, F.; Santos, L.; Abid, Y.; Chaabouni, S. Opt. Mater. 2019,**89**, 355–360.
72 Varshni, Y. P. Physica 1967, **34**(1), 149–154.
73 Kumarasamy, E.; Sanders, S. N.; Tayebjee, M. J. Y.; Asadpoordarvish, A.; Hele, T. J. H.; Fuemmeler, E. G. et al. J. Am. Chem. Soc. 2017, **139**, 12488−12494.
74 Grozema, F. C.; Felter, K. M. J. Phys. Chem. Lett. 2019, **10**, 7208−7214.
75 Yago, T.; Wakasa, M. Chem. Phys. Lett. 2018, **695**, 240–244.
76 Jadhav, P. J.; Mohanty, A.; Sussman, J.; Lee, J.; Baldo, M. A. Nano Lett. 2011, **11**(4), 1495–1498.
77 Dexter, D. L. J.Chem. Phys. 1953, **21** (5), 836−850.
78 Sanders, S. N., Pun, A. B., Parenti, K. R., Kumarasamy, E., Yablon, L. M., Sfeir, M. Y., Campos, L. M. Chem. Sci. 2019, **5**, 1988–2005.
79 Pun, A. B.; Sanders, S. N.; Kumarasamy, E.; Sfeir, M. Y.; Congreve, D. N.; Campos, L. M. Adv. Mater. 2017, **29**(41), 1701416.
80 Pace, N. A.; Zhang, W.; Arias, D. H.; McCulloch, I.; Rumbles, G.; Johnson, J. C. J. Phys. Chem. Lett. 2017, **8**(24), 6086–6091.

For Table of Contents Only